

A mathematical model of intercellular signaling during epithelial wound healing

Filippo Posta

*Dept. of Biomathematics, UCLA, Los Angeles, CA 90095-1766**

Tom Chou

Dept. of Biomathematics, UCLA, Los Angeles, CA 90095-1766 and*

Depts. of Biomathematics and Mathematics, UCLA, CA 90095†

(Dated: November 15, 2021)

Recent experiments in epithelial wound healing have demonstrated the necessity of Mitogen-activated protein kinase (MAPK) for coordinated cell movement after damage. This MAPK activity is characterized by two wave-like phenomena. One MAPK “wave” that originates immediately after injury, propagates deep into the cell layer, and then rebounds back to the wound interface. After this initial MAPK activity has largely disappeared, a second MAPK front propagates slowly from the wound interface and continues into the tissue, maintaining a sustained level of MAPK activity throughout the cell layer. It has been suggested that the first wave is initiated by reactive oxygen species (ROS) generated at the time of injury. In this paper, we develop a minimal mechanistic diffusion-convection model that reproduces the observed behavior. The main ingredients of our model are a competition between ligand (e.g., Epithelial Growth Factor) and ROS for the activation of Epithelial Growth Factor Receptor (EGFR) and a second MAPK wave that is sustained by stresses induced by the slow cell movement that closes the wound. We explore the mathematical properties of the model in connection with the bistability of the MAPK cascade and look for traveling wave solutions consistent with the experimentally observed MAPK activity patterns.

PACS numbers: 87.10.Ed, 87.17.Aa.

Introduction

Coordinated cell movement is an essential feature of many biological processes, such as wound healing, embryonic morphogenesis, and tumor growth¹. In wound healing, cell migration and cell contraction are the two main mechanisms responsible for wound closure. Cell contraction is the dominant mechanism in the closing of small wounds through the so called “purse-string” process². For larger wounds, cell contraction is not sufficient, and surrounding cells must migrate to close larger wounds. While the two mechanisms are not mutually exclusive, there are cases where cell migration is the only healing process³, such as when a strip of cells from an epithelial layer is removed⁴. Despite the existence of experimental assays targeting cell migration during wound healing, there are still many open questions. For instance, before injury, the cells are resting, but after wounding they become motile. What mechanical and biochemical phenomena regulate motility? Is it the availability of free space that leads cells to move toward wound closure? What determines the speed of cell migration? To be able to answer these questions, we need to understand both the mechanical and biochemical aspects of cell migration, and how they might regulate each other. While the physical mechanisms of cell movement have been well-studied^{3,5,6,7}, the complex regulation of the wound healing process by biochemical signals and feedback pathways remains poorly understood. Recent experimental investigations of wounds in epithelial tissue have highlighted novel properties of the intercellular signaling necessary for healing^{8,9}.

Matsubayashi *et al.* (2004) analyzed wounded epithelial monolayers of Madin-Darby canine kidney (MDCK) cells and showed coordinated movement not only by the cells at the wound edge, but by several rows of adjacent cells. In their experiments, cell proliferation did not play a significant role. Their study also showed that the cellular response of the epithelial monolayer is qualitatively characterized by two wave-like activation patterns of ERK 1/2, a Mitogen Activated Protein Kinase (MAPK). These “waves” are characterized by a time-dependent front of higher ERK 1/2 concentration that initiates at the wound edge and spreads into the cell layer. The first rebounding wave-front propagates into the tissue and back to the wound quickly, the second wave-front is slow and sustains MAPK activity in the tissue until wound closure. This second, final wave appears to be related to cell migration through a positive feedback loop, since inhibition of the second MAPK wave halts coordinated cell movement. Moreover, during this second “wave”, MAPK is inactive around the healing edges of the injured layer, but still active in the migrating cells around the open wound⁸.

Nikolić *et al.* (2006) extended the experimental analysis in⁸ by probing the epithelial wound healing assay with a novel wound generating technique. They used polydimethylsiloxane (PDMS) slabs to create two different wounding protocols. A peel-off injury is created by growing part of the epithelial monolayer over a PDMS slab. Once the slab is peeled-off, taking with it the cells grown over the PDMS, it creates a wound that breaks some cells at the wound edge, but leaves the space surrounding the wound free of cellular debris. The other protocol consists of the removal of a PDMS slab that

forms the boundary of the cellular monolayer, its removal leaves intact the cells in direct contact with the slab, but now provides free space at one edge of the monolayer. This “unconstraining” protocol avoids cell tearing upon PDMS removal. Experimenting with these two techniques, and with the standard scratch wound assay, the authors confirmed the presence of two separate waves of MAPK in case of injury. The unconstraining experiments expressed only the slow, final wave. In this case, cell movement was limited and random, suggesting that availability of free space is not enough to generate an organized migration of the epithelial layer and that mechanical injury is necessary. Accordingly, scratch and peel-off experiments resulted in both waves of MAPK activation and in collective monolayer migration. Using immunofluorescence, Nikolić *et al.* (2006) were also able to identify reactive oxygen species (ROS) as one of the key components of the intercellular signaling responsible for the observed pattern of MAPK activation. They discovered that ROS are generated immediately after injury and remain present around the wound edge for at least the duration of the first rebounding wave. Inhibition of ROS by N-acetyl-L-cysteine resulted in the absence of both MAPK waves and cell migration. The results from the two studies^{8,9} are summarized in Table I.

In this paper, our aim is to build a mathematical model that reproduces an that can be used to analyze the properties of MAPK activation during wound healing experiments. Because of its relevance and ubiquity, the MAPK pathway remains the subject of many computational and mathematical modeling studies¹⁰. The MAPK cascade is a signal transduction pathway that relays an external stimulus to the cell, it is characterized by the sequential activation of three protein kinases¹¹. Huang and Ferrell¹² proposed a system of 18 differential equations representing the 10 reactions that compose the three-kinase MAPK cascade. A mathematical and computational analysis of the system showed that the cascade has the effect of amplifying an input signal (e.g., receptor phosphorylation) in such a way that its overall behavior can be compared to that of a cooperative enzyme¹³. These first computational studies sparked additional modeling efforts that, coupled with ongoing discoveries by experimentalists, have led to many more advanced models that exhibit characteristics (e.g., bistability, ultrasensitivity, oscillations, etc.) of the MAPK signaling pathway^{14,15,16,17}.

Here, we are not interested in the intracellular dynamics of MAPK, but rather on its role within the wound healing signaling network. For this reason, we will treat the MAPK cascade as a black box, using the results in^{11,18} to essentially represent the whole cascade as a switch for signal transmission. In this approach, MAPK/ERK is the output of the “signaling switch”. ROS are one input that can activate the switch, but are unlikely to be the only one because of the different properties of the two activation waves. As suggested in⁹ and in other wound healing experiments^{19,20}, other in-

Experiment	Results
Scratch wound	Two MAPK waves, cell migration
Closed wound	No MAPK activity, no cell movement
MAPK inhibition	No MAPK waves, no cell migration
Slow wave inhibition	No cell migration
Peel-off wound	Two MAPK waves, cell migration
Unconstraining	Slow, second wave only, no cell migration
ROS inhibition	No MAPK waves, no cell migration

TABLE I: Summary of the experimental results from^{8,9}.

puts are diffusible ligands and their cell receptors. For instance, Epidermal Growth Factor (EGF) and EGF Receptor (EGFR) play essential roles in promoting cell migration, proliferation and wound closure^{21,22}. Moreover, positive and negative feedbacks between EGFR signaling and the MAPK cascade have been demonstrated experimentally and verified computationally^{23,24,25}. Although Nikolić *et al.* suggest EGF as a possible signal, as well as other molecules, they did not pursue the topic in their work. However, they did identify Reactive Oxygen Species (ROS) as direct regulator of MAPK activity in their wound healing experiments. Since ROS have been shown to induce EGFR activation in the absence of EGF²⁶, this finding is in agreement with other studies that showed the regulatory role of ROS in wound healing^{27,28} and MAPK signaling^{29,30}.

Because of the documented connection between diffusible signals, wound healing and MAPK activation, we propose a mechanistic model based on ligand-mediated intercellular signaling that reproduces the observed MAPK activation pattern, and that is consistent with the qualitative experimental features listed in Table I.

Mathematical Model

The experimental results from^{8,9} provide evidence of spatio-temporal MAPK signaling for the regulation of cell migration during wound healing, without determining the exact biochemical events that govern it. The fact that free space by itself is not enough to produce coordinated cell migration suggests that ROS is not the only diffusible signal needed to generate the two waves of MAPK activation. To explain the observed spatio-temporal MAPK pattern, at least two diffusible signals are needed. Both ROS and EGF molecules are able to diffuse in the extracellular space (ROS can also move across the cell membrane) and both can phosphorylate the EGF membrane receptor (EGFR), activating the MAPK cascade. EGF induces phosphorylation of the cytoplasmic tail of EGFR by binding to it. Reynolds *et al.* (2003)

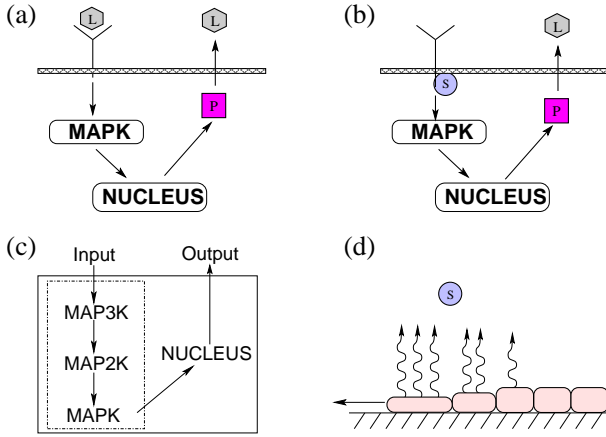


FIG. 1: Schematic of biophysical events during wound healing. (a) diffusible ligands (L) phosphorylate membrane receptors by binding to them, activating the MAPK cascade that leads to the production of intracellular protease (P). Protease induces ligand release. (b) ROS (S) can also interact with membrane receptors by inducing phosphorylation of their cytoplasmic tail, which also activates the MAPK cascade and promotes release of ligands into the extracellular matrix. Diffusible ligand and ROS represent two independent triggers of the MAPK cascade. (c) Schematic of the three-kinase cascade that characterizes MAPK signaling. (d) The stresses caused by cell movement toward wound closure can lead to ROS release^{29,32,33}.

showed that ROS can induce EGFR phosphorylation even in the absence of EGF by binding to intracellular phosphatases. Also well documented is the positive feedback between EGF and the MAPK cascade, and its ability to produce long range signaling through autocrine relays³¹. Finally, ROS can be generated by mechanical

stresses like the ones generated by migration of the epithelial monolayer²⁹, thus providing a feedback loop between MAPK activation, cell motility, and further ROS production. These four signaling mechanisms are summarized in Fig. 1 and constitute the foundation of our mathematical model.

The wound healing system is a three-dimensional one, and the migration of individual cells toward wound closure is not exactly normal to the wound edge as shown by cell tracking experiments⁹. Here, we simplify the analysis by considering the cell layer in cross section as a semi-infinite straight line, with the wound initially positioned at the origin. The resulting two-dimensional system consists of a semi-infinite cell layer that is immersed in medium of infinite height (the medium in⁹ is 3mm which is much larger than any other length scale in the problem). We model four species: ROS, one diffusible ligand (*e.g.*, EGF), one ligand receptor (*e.g.*, EGFR) and playing the role of the output of the MAPK cascade “black box”, a protease that is the intracellular precursor of the ligand (*e.g.*, the piece completing the feedback loop between EGF and the MAPK cascade in Figs. 1-(a) and 1-(b)). We denote the local concentrations of these species by L , S , R , and P respectively. As depicted in Fig. 1, the signal can be transmitted to the cell in two different ways: through a ligand-receptor complex ($C_L \equiv R \cdot L$) and a ROS-receptor complex³⁸ ($C_S \equiv R \cdot S$). We will assume that the number of available cell membrane receptors is in excess, implying that R is approximately constant and that ROS-ligand-receptor complexes are negligible.

A schematic representation of the system is given in Fig. 2. The governing equations and boundary conditions of our model are

$$\frac{\partial L(X, Z, T)}{\partial T} = D_L \left(\frac{\partial^2 L(X, Z, T)}{\partial X^2} + \frac{\partial^2 L(X, Z, T)}{\partial Z^2} \right), L(X, Z = \infty, T) = 0, \quad (1)$$

$$D_L \frac{\partial L(X, 0, T)}{\partial Z} = k_{\text{on}}^L RL(X, 0, T) - k_{\text{off}}^L C_L(X, T) - g_L P(X, T), \quad (2)$$

$$\frac{\partial C_L(X, T)}{\partial T} = k_{\text{on}}^L RL(X, 0, T) - (k_{\text{off}}^L + k_{\text{ec}}^L) C_L(X, T), \quad (3)$$

$$\frac{\partial S(X, Z, T)}{\partial T} = D_S \left(\frac{\partial^2 S(X, Z, T)}{\partial X^2} + \frac{\partial^2 S(X, Z, T)}{\partial Z^2} \right), S(X, Z = \infty, T) = 0, \quad (4)$$

$$D_S \frac{\partial S(X, 0, T)}{\partial Z} = k_{\text{on}}^S RS(X, 0, T) - g_S \Pi_S(C_L, X, T), \quad (5)$$

$$\frac{\partial C_S(X, T)}{\partial T} = k_{\text{on}}^S RS(X, 0, T) - k_{\text{ec}}^S C_S(X, T), \quad (6)$$

$$\frac{\partial P(X, T)}{\partial T} = -k_P P(X, T) + g_P \Pi_P(C_L, C_S). \quad (7)$$

Equations (1) and (4) describe the diffusion of ligands

and ROS in the extracellular medium with homogeneous

diffusion constant D_L and D_S , respectively. Eqn. (2) accounts for the flux of ligand across the surface of the cellular layer including ligand-receptor complex formation with rate constant k_{on}^L , ligand-receptor complex dissociation with rate constant k_{off}^L , and extracellular ligand release by intracellular protease with rate g_L . Eqn. (3) governs the kinetics of ligand-receptor complexes, with new complexes forming at rate k_{on}^L and dissociating with rate k_{off}^L , k_{ec}^L represents the rate of receptor-mediated endocytosis of the ligand-bound receptor complexes. Eqn. (5) describes the diffusive flux of ROS due to formation of ROS-receptor complexes with rate k_{on}^S and to ROS production by the functional $\Pi_S(C_L, X, T)$. The kinetics of ROS-receptor complexes is represented by Eqn. (6) and its terms are analogous to the ones in Eqn. (3), except that there is no ROS release from the ROS-receptor complex in accordance with²⁶. The last equation describes the cellular response to extracellular signaling through the activity of intracellular proteases. Within the wound healing framework, protease activity is directly related to ERK1/2 activity measured in⁹. In particular, the protease dynamics is characterized by a degradation term with rate constant k_P and a source term $\Pi_P(C_L, C_S)$ with maximum production rate g_P . To complete the description of the mathematical model, we need to impose reasonable functional forms for Π_P and Π_S .

The role of the functional $\Pi_P(C_L, C_S)$ is to represent the intermediate biochemical steps that lead to protease production. These steps include the MAPK cascade and any other reaction in the feedback loop between ligand binding and ligand release (*e.g.*, the solid box in Fig. 1-(c)). In the literature, Π_P is usually represented as a sigmoidal function of cell surface complexes such as the Hill function^{11,18,34}. If the level of receptor signaling is given by the total concentration of complexes ($C_L + C_S$), we propose the following functional form:

$$\Pi_P(C_L, C_S) = \frac{(C_L + C_S)^n}{C_A^n + (C_L + C_S)^n}, \quad (8)$$

where n is an effective Hill coefficient, and C_A represents an activation threshold of the signaling pathway.

Defining the ROS source Π_S is more problematic since the experimental evidence suggests an interplay between cellular signaling and cell migration, thus involving mechanical forces whose description goes beyond the scope of this paper. Conversely, the production of ROS due to wound induction is embedded in the initial conditions of the system and it is not described in Π_S . Generally, ROS production increases with cell metabolism²⁹. In our case, metabolic increase may be related to cells becoming motile^{29,33} and/or to ligand signaling³². We use a Hill function multiplied by a decaying exponential to represent Π_S :

$$\Pi_S(C_L, X, T) = \begin{cases} 0 & T < T_D \\ \frac{(C_L(X, T - T_D))^m}{S_A^m + (C_L(X, T - T_D))^m} e^{-k_x X} & T \geq T_D \end{cases}. \quad (9)$$

The Hill functional represents ligand-mediated ROS production stemming from the phosphorylation of a receptor's tail during ligand binding. The delay T_D represents the delay between ligand binding and ROS production. Finally, the exponential factor in Eqn. (9) describes reduction in ROS production due to the decrease in motility from cells near the wound edge ($X = 0$) to cells farther from it.

Upon introducing the following dimensionless quantities

$$t = k_P T, \quad x = X \sqrt{\frac{k_P}{D_L}}, \quad z = Z \sqrt{\frac{k_P}{D_L}},$$

$$l = L \frac{k_P k_{\text{ec}}^L k_{\text{on}}^L R}{g_L g_P (k_{\text{off}}^L + k_{\text{ec}}^L)}, \quad c_L = C_L \frac{k_P k_{\text{ec}}^L}{g_L g_P}, \quad c_S = C_S \frac{k_{\text{ec}}^S}{g_S},$$

$$s = S \frac{k_{\text{on}}^S R}{g_S}, \quad p = P \frac{k_P}{g_P},$$

we express the system of equations in dimensionless form:

$$\frac{\partial l(x, z, t)}{\partial t} = \frac{\partial^2 l(x, z, t)}{\partial x^2} + \frac{\partial^2 l(x, z, t)}{\partial z^2}, \quad (10)$$

$$\alpha l_z(x, 0, t) = l(x, 0, t) - \beta [l(x, 0, t) - c_L(x, t)] - p(x, t), \quad (11)$$

$$\varepsilon \frac{\partial c_L(x, t)}{\partial t} = l(x, 0, t) - c_L(x, t), \quad (12)$$

$$\delta \frac{\partial c_S(x, t)}{\partial t} = s(x, 0, t) - c_S(x, t), \quad (13)$$

$$\frac{\partial s(x, z, t)}{\partial t} = \eta \left(\frac{\partial^2 s(x, z, t)}{\partial x^2} + \frac{\partial^2 s(x, z, t)}{\partial z^2} \right), \quad (14)$$

$$\nu s_z(x, 0, t) = s(x, 0, t) - \pi_s(c_L, x, t), \quad (15)$$

$$\frac{\partial p}{\partial t} = -p + \pi_p(c_L, c_S), \quad (16)$$

where the dimensionless parameters are

$$\alpha = \frac{\sqrt{D_L k_P} (k_{\text{off}}^L + k_{\text{ec}}^L)}{k_{\text{on}}^L R k_{\text{ec}}^L}, \quad \beta = \frac{k_{\text{off}}^L}{k_{\text{ec}}^L}, \quad \delta = \frac{k_P}{k_{\text{ec}}^S}, \quad (17)$$

$$\varepsilon = \frac{k_P}{k_{\text{off}}^L + k_{\text{ec}}^L}, \quad \eta = \frac{D_S}{D_L}, \quad \nu = \sqrt{\frac{k_P}{D_L}} \frac{D_S}{k_{\text{on}}^S R}.$$

The parameters α and ν characterize the relative rates of diffusion and binding, while β represents the strength of complex degradation relative to ligand dissociation. The parameters ε and δ describe the speed of binding and endocytosis relative to ligand release mediated by intracellular species, and η is the ratio of diffusivity between ROS and EGF ligand.

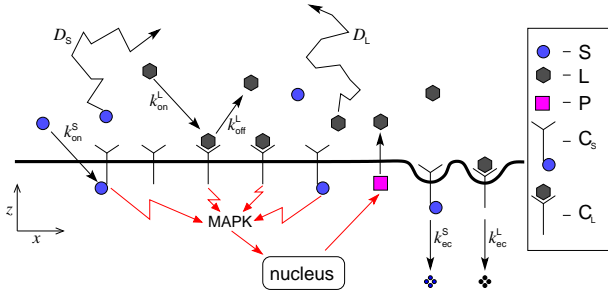


FIG. 2: Schematic of simplified signaling pathway during wound healing: ligands (L) and ROS (S) are free to diffuse and bind to cell surface receptors. This binding forms complexes (C_S and C_L) that activate MAPK signaling. Complexes are lost due to endocytosis or, in the case of ligand-receptor complexes, through ligand unbinding and endocytosis. Intracellular proteases (P) release extracellular ligands (L).

The dimensionless protease and ROS production functions become

$$\pi_p(c_L, c_S) = \frac{(c_L + \gamma c_S)^n}{c_A^n + (c_L + \gamma c_S)^n}, \quad (18)$$

$$\pi_s(c_L, x, t) = \begin{cases} 0 & t < \tau \\ \frac{(c_L(x, t - \tau))^m}{s_A^m + (c_L(x, t - \tau))^m} e^{-\lambda x} & t \geq \tau \end{cases}, \quad (19)$$

where $c_A = C_A(k_P k_{ec}^L)/(g_L g_P)$, $\gamma = (g_S k_P k_{ec}^L)/(g_L g_P k_{ec}^S)$, $\tau = T_D k_P$, $\lambda = k_x L$, and $s_A = (S_A k_P k_{ec}^L)/(g_L g_P)$.

Fast Binding Approximation

Before we proceed to the analysis of the model, we are going to make an assumption that significantly simplifies the model and that is also justifiable biophysically. We assume that ligand dissociation and complex degradation is fast compared to protease degradation, *e.g.*, $k_P \ll k_{ec}^S, k_{off}^L, k_{ec}^L$. In this limit, ε and δ are small and Eqns. (12) and (13) can be treated as a singular perturbation. On timescales of protease degradation the concentration of ligand-receptor and ROS-receptor complexes are approximately that of the surface concentration of free ligand and ROS, respectively. If we consider only the “outer” solutions of Eqns. (12) and (13), our full model reduces to the three equations:

$$\frac{\partial l(x, z, t)}{\partial t} = \frac{\partial^2 l(x, z, t)}{\partial x^2} + \frac{\partial^2 l(x, z, t)}{\partial z^2}, \quad (20)$$

$$\alpha l_z(x, 0, t) = l(x, 0, t) - p(x, t), \quad (21)$$

$$\frac{\partial s(x, z, t)}{\partial t} = \eta \left(\frac{\partial^2 s(x, z, t)}{\partial x^2} + \frac{\partial^2 s(x, z, t)}{\partial z^2} \right), \quad (22)$$

$$\nu s_z(x, 0, t) = s(x, 0, t) - \pi_s(l, x, t), \quad (23)$$

$$\frac{\partial p}{\partial t} = -p + \pi_p(l, s), \quad (24)$$

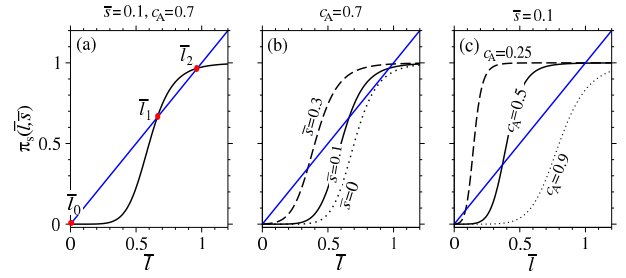


FIG. 3: Steady state configurations. (a) Graphical solution of Eqn. (26) for $\bar{s} = 0.1$, and $c_A = 0.7$. There are three solutions representing two stable steady states (\bar{l}_0 and \bar{l}_2) and one unstable equilibrium (\bar{l}_1). (b) If we fix the activation threshold ($c_A = 0.7$), different values of ROS concentration lead to different steady state configurations. Bistability is possible if there is enough ROS, otherwise the only stable steady state is the one with no MAPK activity. (c) We fix ROS concentration to $\bar{s} = 0.1$ and graphically solve Eqn. (26) for different values of c_A . Bi-stability can arise only if the activation threshold is sufficiently small. The Hill coefficient $n = 8$ was used in all plots.

where all functions now represent “outer” solutions valid at times beyond initial transients in complex formation. We verified that this approximation holds throughout all of the analysis performed in the next section.

Analysis & Results

The spatio-temporal MAPK activation patterns can arise from different mechanisms. For example, one (or more) activation pattern could consist of a traveling front connecting two stable steady states, corresponding to high and low MAPK concentrations. In this section we describe the steady states of the system of Eqns. (20)-(24) and present an overview of the qualitative behavior of the solutions of the model. After establishing the dynamics of the mathematical model, we use the known model parameters to determine the nature of the MAPK patterns and some of their properties.

The complexity of our model requires analysis through numerical simulations. For this purpose we use an explicit finite difference scheme that is forward in time and centered in space, implemented in Fortran. We use a uniform grid discretization along the direction of the cell layer (*e.g.*, x) and a geometrical grid discretization along the direction normal to the cell layer (*e.g.*, z) to maximize accuracy and minimize run-time. This approach and its advantages have been previously described in³⁵.

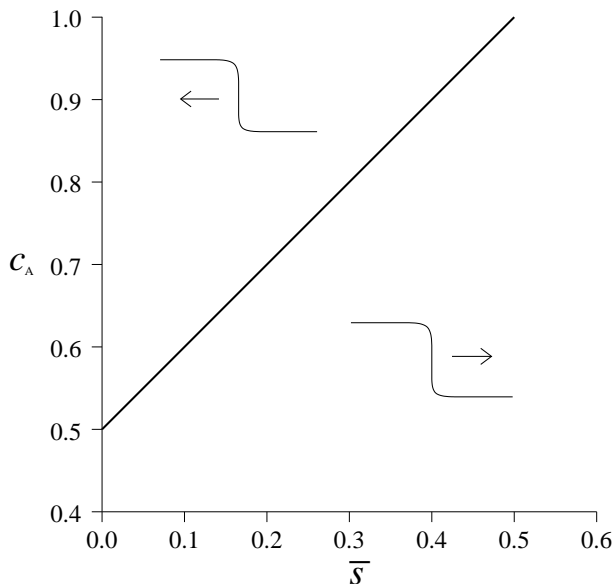


FIG. 4: Traveling waves connecting the state of MAPK activation and the state of MAPK inactivity can move toward or away from the wound depending on ROS concentration at cell layer level (\bar{s}) and activation threshold (c_A) when $n \rightarrow \infty$. The thick black line indicates conditions under which the front is not moving. Regimes above the line lead to traveling waves moving toward the wound, while those below the line lead to fronts moving away from the wound.

Steady States & Traveling Fronts

The steady states of the model in Eqs. (20)-(24) satisfy:

$$\bar{l} = p, \quad \bar{s} = \pi_s(\bar{l}, x, t), \quad \text{and} \quad p = \pi_p(\bar{l}, \bar{s}), \quad (25)$$

where the overbar indicates that the value of ligand or ROS concentration is taken at $z = 0$ (e.g., $\bar{l} = l(x, z = 0, t)$). The resulting condition

$$\bar{l} = \pi_p(\bar{l}, \bar{s}) \quad (26)$$

is always satisfied by the trivial solution ($\bar{l} = 0, \bar{s} = 0$), but under certain conditions it can have two more solutions as highlighted in Fig. 3-(a). In this case the three roots are two stable steady states, \bar{l}_0 and \bar{l}_2 , and an unstable one, \bar{l}_1 . The two stable steady states represent a state of no ligand signaling, $\bar{l}_0 = 0$, and a state of active ligand signaling, $\bar{l}_2 > 0$, respectively. From Fig. 3 we can also infer how ROS concentration \bar{s} and the activation threshold c_A control the steady states of the system. If we fix the activation threshold at a sufficiently high value, the system attains only the trivial steady state, $\bar{l} = \bar{l}_0 = 0$, unless there is enough ROS to sustain the signaling pathway, as shown in Fig. 3-(b). Conversely, if we fix \bar{s} , the system will be bistable only if the activation threshold c_A is sufficiently small (Fig. 3-(c)).

Bistability implies that the model admits traveling front solutions connecting the two stable steady states.

We can approximate the front speed analytically by considering a simpler scenario in which the concentration of ROS at cell layer level, \bar{s} , is constant and take the limit $n \rightarrow \infty$ for the Hill coefficient of π_p . In this limit, the sigmoidal protease production function π_p equals the Heaviside function centered at $c_A - \bar{s}$:

$$\lim_{n \rightarrow \infty} \pi_p(\bar{l}, \bar{s}) = H(\bar{l} + \bar{s} - c_A) = \begin{cases} 1 & \bar{l} \geq c_A - \bar{s} \\ 0 & \bar{l} < c_A - \bar{s} \end{cases}. \quad (27)$$

In this limit the system is bistable for $0 < c_A - \bar{s} < 1$, and the roots of Eqn. 26 are $\bar{l}_0 = 0$, $\bar{l}_1 = c_A - \bar{s}$, and $\bar{l}_2 = 1$. Furthermore, we can determine the velocity and direction of the traveling fronts by proceeding as in³⁶, obtaining:

$$c_A - \bar{s} = \frac{1}{\pi} \int_{\alpha v}^{\infty} \frac{\alpha \sqrt{q^2 - vq}}{q(1 + vq)(\alpha^2 q^2 - \alpha^2 vq + 1)} dq, \quad (28)$$

which gives an implicit relation for v , the velocity of the traveling wave for a fixed concentration of ROS. The integration variable q in the above integral arises from the Fourier transformation used to derive Eqn. 28. From Eqn. 28 we find that the front velocity is a monotonically increasing function of the parameter α (see Eqn. 17). This result is expected since an increase in α corresponds to either an increase in ligand diffusivity or a decrease in ligand binding, and both changes result in the front reaching farther distances in a shorter amount of time. The direction of the front is determined by the threshold $c_A - \bar{s}$. If $c_A - \bar{s} < 1/2$, the front of active MAPK will move away from the wound, and deep into the cell layer. If $c_A - \bar{s} > 1/2$, MAPK activity will recede toward the wound. Regimes that delineate forward and backward traveling MAPK waves are indicated in Fig. 4. These results provide useful insight for the general case of $n < \infty$ and diffusing ROS. Numerical simulations show that for Hill coefficient as low as $n = 6$, the instantaneous front velocity is within 10% of that obtained from Eqn. 28. To summarize, we showed that the system can have two stable steady states and that traveling wave solutions connecting them are possible. In particular, ROS can determine the existence, velocity and direction of the fronts by effectively regulating the activation threshold of the MAPK cascade.

ROS/EGF regulation of MAPK activation

Bistability is necessary but not sufficient for the existence of traveling wave solutions. In this section we explore the parameter space of the wound healing assay to determine the nature of the MAPK fronts observed in^{8,9}. To avoid ambiguity, we divide the MAPK dynamics during wound healing into three wave-like events. The first event corresponds to the fast activation of MAPK initiated by the wound. It lasts until the activation front

Parameter	Typical Value	Ref.
D_L	$10^{-8} - 10^{-6} \text{ cm}^2 \text{ s}^{-1}$	31
k_{on}^L	$10^{-15} - 10^{-12} \text{ cm}^3 \text{ s}^{-1}$	31
k_{off}^L	$10^{-3} - 10^{-2} \text{ s}^{-1}$	31
k_{ec}^L	$10^{-3} - 10^{-2} \text{ s}^{-1}$	31
k_P	$10^{-4} - 10^{-3} \text{ s}^{-1}$	31
R	$10^{10} - 10^{13} \text{ cm}^{-2}$	31
g_P	$0.17 \times 10^8 \text{ cm}^{-2} \text{ s}^{-1}$	36
g_L	$0.54 \times 10^{-2} \text{ s}^{-1}$	37
C_A	10^9 cm^{-2}	37

TABLE II: Typical values of model parameters.

reaches its maximum depth in the cell layer. The second event is characterized by decrease of MAPK activity. It moves from deep into the epithelial monolayer toward the wound. These first two events qualitatively correspond to the first “rebounding wave” observed in the experiments^{8,9}. The last event consists of a slow activation front that starts at the wound edge and moves away from the wound. This last “wave” is initiated when the cells in the layer start moving to close the wound itself, and is sustained when the wound is large, preventing closure in finite time⁹.

To reproduce the observed MAPK dynamics, we numerically integrated Eqns. (20)-(24) using the ligand related parameters given in Table II. Although we could not find analogous references for physical parameters of ROS, we estimated parameter values from various sources. We used the self-diffusivity of water together with the Einstein relation to bound the value of η between 10 and 100. From the results in²⁶ it seems reasonable to assume $k_{\text{ec}}^S \approx k_{\text{ec}}^L$. We assume that the initial concentration of ligand and protease is zero, while the concentration of ROS is represented by a narrow Gaussian with width equal to the size of a single cell; it represents the ROS initially released by cell rupture. Our numerical results are summarized in Figs. 5 and 6. Fig. 5 compares the time evolution of the distance of the front from the wound as predicted by Eqns.(20)-(24) with the experimental values observed in⁹ for scratch wounds. The position of the front is determined by evaluating the inflection point of protease concentration after each time step. The model is able to replicate the observed MAPK behavior and we used it to investigate the dynamics of the three activation wave-like patterns. Fig. 6 shows the time evolution of the profiles of the three MAPK “waves”. The first wave (Fig. 6-(a)) is driven by ROS production at the onset of wound and its fast diffusion. However, there is not enough ROS for either ligand or protease concentration to reach the signaling steady state (e.g., $p = \bar{l} = 1$). As a result, the first “wave” can only propagate as far as $\sim 480 \mu\text{m}$ before receding. As ROS diffuses away, protease concentrations decrease (Fig. 6-(b)) until the cells start to move (after about 30

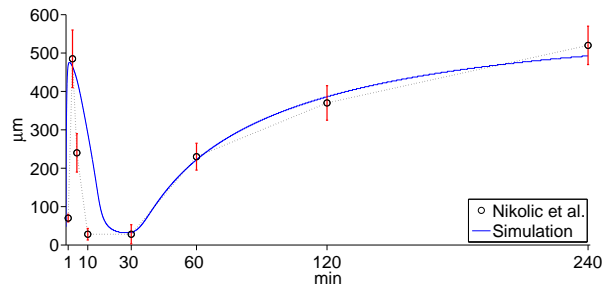


FIG. 5: Time evolution of the distance from the wound edge of the MAPK front. The circles and the intersecting vertical bars represent the average front position and one standard deviation error bars, respectively. Their values have been obtained from the experimental data in⁹. The solid trace has been obtained through a computer simulation of Eqns. (20)-(24) with dimensionless parameters: $\alpha = 0.35$, $\eta = 16$, $\nu = 5$, $c_A = 0.625$, $n = 6$, $\gamma = 2$, $p_A = 0.975$, $m = 9$, $\lambda = 0.55$, $\tau = 2.56$. These parameters are based on $k_P = 5.6 \times 10^{-3} \text{ s}^{-1}$, $D_L = 5.6 \times 10^{-7} \text{ cm}^2 \text{ s}^{-1}$, $k_{\text{ec}}^L = k_{\text{off}}^L = 10^{-2} \text{ s}^{-1}$, $g_L = 0.54 \times 10^{-2} \text{ s}^{-1}$, $g_P = 0.17 \times 10^8 \text{ cm}^{-2} \text{ s}^{-1}$, $R = 3.2 \times 10^{11} \text{ cm}^{-2}$, $k_{\text{on}}^L = 10^{-15} \text{ cm}^3 \text{ s}^{-1}$, $C_A = 10^9 \text{ cm}^{-2}$.

minutes from injury). At that time, ROS is produced by the moving cells and fuels the positive feedback loop between ligand and protease. The nonlinear effects of π_P allow protease levels to increase until they reach a signaling steady-state. At this point, the front moves like a true traveling-wave (Fig. 6-(c)), with its speed and distance traveled regulated by the ROS source function π_S . We can also track the time-evolution of the variables in the model. Fig. 6-(d) shows how protease concentration at the wound edge $x = 0$ changes in time. From this graph we observe that during the first MAPK event the protease concentration never reaches the “signaling” steady-state $p \approx 1$ and eventually decreases. During the third wave, protease concentration reaches the “signaling” steady-state and remains there as shown by the flat part of the graph in Fig. 6-(d). To summarize, only the third MAPK front behaves as a true traveling wave, while the initial two events (corresponding to the first “rebounding wave” observed in experiments) are actually transient, diffusion-driven patterns.

Conclusions

We have formulated a mathematical model for the dynamics of intercellular signaling observed during wound healing experiments. From this model, we were able to replicate the signaling patterns observed in^{8,9}, and to provide insight regarding their nature. Our choice of EGF as signaling ligand is based upon literature review, but lacks experimental evidence within the epithelial wound healing assay. However, we showed that the properties of EGF (and EGFR) fit the profile for the

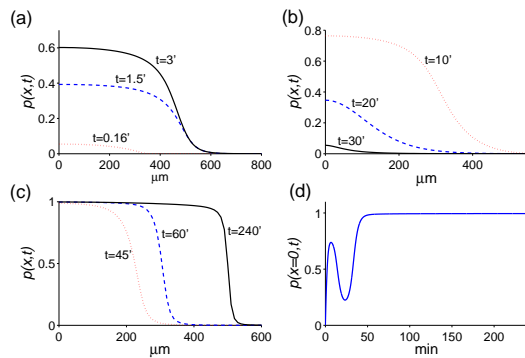


FIG. 6: Time evolution of protease. (a) After injury, the fast diffusion of ROS drives MAPK activation. (b) As ROS diffuses away, the positive feedback loop between MAPK and ligand is not strong enough to sustain signaling and the depth of the front decreases. (c) Once the cells start moving, ROS production and the ligand-protease feedback loop fuel the activation front. (d) Time evolution of protease concentration at $x = 0$. The parameters used to obtain these plots are the same as the ones used to generate Fig. 5.

unidentified diffusible signals mentioned in⁹. Our model can be expanded to incorporate other diffusible signaling molecules. Although it may be possible to find physiologically realistic sets of parameters that lead to signaling patterns consisting of three separate traveling waves, the parameters associated with the EGF/ROS/MAPK system lead to only one final traveling wave. The first two

notable events being described by purely diffusive and decays dynamics, respectively.

An aspect of our current model that needs improvement and further analysis is the determination of the ROS source function Π_S . From the experiments in⁹, this term seems to be negligible since they only detected the presence of extracellular ROS up to ~ 10 min after wounding. However, there is substantial evidence indicating that cell motility and ligand-receptor binding can induce ROS production. A plausible explanation for these conflicting results could be that ROS produced after wounding is fully recaptured by intracellular processes (including EGFR phosphorylation) and never crosses the cell membrane. Nonetheless, we performed many numerical tests and found that if $\Pi_S = 0$ (data not shown), then all three MAPK events are diffusion driven and the signaling pattern is due to the different diffusion properties of ROS and ligand (EGF). A more physically realistic approach might be to include the mechanical events that take place within the cell layer and the reaction that lead to ROS production after ligand binding. Such an approach could provide important insights about the mechanisms of post-wound ROS production and their relevance within the MAPK signaling context.

Acknowledgments

We thank M. Gibbons, S. Shvartsman, and C. Muratov for useful discussion. This work was supported by NSF grant DMS-0349195 and NIH grant K25 AI58672.

* fposta@ucla.edu

† tomchou@ucla.edu

- 1 P. Martin and S. Parkhurst, *Development* **131**, 3021 (2004).
- 2 D. Kiehart, *Curr. Biol.* **9**, R602 (1999).
- 3 J. Sherratt and J. Murray, *Proc. Roy. Soc. Lond.* **241**, 29 (1990).
- 4 M. Poujade, E. Grasland-Mongrain, A. Hertzog, J. Jouanneau, P. Chavrier, B. Ladoux, A. Buguin, and P. Silberzan, *PNAS* **104**, 15988 (2007).
- 5 P. DiMilla, K. Barbee, and D. Lauffenburger, *Biophys. J.* **84**, 2907 (1991).
- 6 J. Murray, *Mathematical Biology II: Spatial Models and Biomedical Applications* (Springer, Berlin, 2003).
- 7 P. Maini, D. McElwain, and D. Leavesley, *Appl. Math. Lett.* **17**, 575 (2004).
- 8 Y. Matsubayashi, M. Ebisuya, S. Honjoh, and E. Nishida, *Curr Biol* **14**, 731 (2004).
- 9 D. Nikolić, A. Boettiger, and J. B. ans S.Y. Shvartsman, *AJP-Cell Physiology* **291**, C68 (2006).
- 10 R. Orton, O. Sturm, V. Vyshemirky, M. Calder, D. Gilbert, and W. Kolch, *Biochem. J.* **392**, 249 (2005).
- 11 J. Ferrell, *Trends Biochem. Sci.* **12**, 460 (1996).
- 12 C. Huang and J. Ferrell, *PNAS* **93**, 10078 (1996).
- 13 J. Keener and J. Sneyd, *Mathematical Physiology* (Springer, Berlin, 1998), ISBN 0-380-98381-3.

- 14 L. Qiao, R. Nachbar, I. Kevrekidis, and S. Shvartsman, *PLoS Comp. Biol.* **3**, 1819 (2007).
- 15 J. Hornberg, B. Binder, F. Bruggeman, B. Schoeberl, R. Heinrich, and H. Westerhoff, *Oncogene* **24**, 5533 (2005).
- 16 B. Schoeberl, C. Eichler-Jonsson, E. Gilles, and G. Muller, *Nature Biotech.* **20**, 370 (2002).
- 17 S. Sasagawa, Y. Ozaki, K. Fujita, and S. Kuroda, *Nat. Cell Bio.* **7**, 365 (2005).
- 18 J. Ferrell, *Trends Biochem. Sci.* **8**, 288 (1997).
- 19 K. Xu, Y. Ding, J. Ling, Z. Dong, and F. Yu, *Inv. Ophthalmol. Vis. Sci.* **45**, 813 (2004).
- 20 E. Block, A. Matella, N. SundarRaj, E. Iszkula, and J. Klarlund, *J. Biol. Chem.* **279**, 24307 (2004).
- 21 H. Wiley, S. Shvartsman, and D. Lauffenburger, *TRENDS Cell Biol.* **13**, 43 (2003).
- 22 E. Joslin, L. Opresko, A. Wells, H. Wiley, and D. Lauffenburger, *J. Cell Sci.* **120**, 3688 (2007).
- 23 S. Santos, P. Verveer, and P. Bastiaens, *Nature Cell Biol.* **9**, 324 (2007).
- 24 B. Kholodenko, *Nat. Rev. Mol. Cell Biol.* **7**, 165 (2006).
- 25 B. Kholodenko, *Nature Cell Biol.* **9**, 247 (2007).
- 26 A. Reynolds, C. Tischer, P. Verveer, O. Rocks, and P. Bastiaens, *Nat. Cell Biol.* **5**, 447 (2003).
- 27 S. Roy, S. Khanna, K. Nallu, T. Hunt, and C. Sen, *Mol. Ther.* **13**, 211 (2006).
- 28 C. Sen and S. Roy, *Biochim. Biophys. Acta* **1780**, 1348

- (2008).
- ²⁹ M. Torres, *Front Biosc.* **8**, 369 (2003).
- ³⁰ J. McCubrey, M. LaHair, and R. Franklin, *Antiox. Redox Sign.* **8**, 1775 (2006).
- ³¹ M. Pribyl, C. Muratov, and S. Shvartsman, *Biophys. J.* **84**, 883 (2003).
- ³² S. Rhee, Y. Bae, S. Lee, and J. Kwon, *Sci. STKE* **53**, pe1 (2000).
- ³³ M. Ali, P. Mungai, and P. Schmacher, *Am. J. Physiol. Lung Cell Mol. Physiol.* **291**, 38 (2006).
- ³⁴ S. Shvartsman, C. Muratov, and D. Lauffenburger, *Development* **129**, 2577 (2002).
- ³⁵ F. Posta, S. Shvartsman, and C. Muratov, *J. Comput. Phys.* **227**, 8622 (2008).
- ³⁶ C. Muratov, F. Posta, and S. Shvartsman, *Phys. Biol.* **6**, 13 (2009).
- ³⁷ M. Pribyl, C. Muratov, and S. Shvartsman, *Biophys. J.* **84**, 3624 (2003).
- ³⁸ ROS are known to activate EGFR by associating with its cytoplasmic tail, and inactivating its phosphatase activity. Kinetically, modeling this process is equivalent to irreversible ROS-EGFR ($C_S \equiv R \cdot S$) complex formation.